Transp Porous Med
DOI 10.1007/s11242-015-0526-5

Pre-asymptotic Transport Upscaling in Inertial and Unsteady Flows Through Porous Media

Nicole Sund[1] · **Diogo Bolster**[1] · **Steven Mattis**[2] · **Clint Dawson**[2]

Received: 15 October 2014 / Accepted: 3 June 2015

Abstract In most classical formulations of flow and transport through porous media Reynolds numbers are assumed to be small (Re $<$ 1), meaning that the role of inertia is considered negligible. However, many examples of practical relevance exist where this is not the case and inertial effects can be important leading to changes in flow structure and even giving rise to unsteady and turbulent flows as Reynolds numbers become larger. This change in flow structure can have a profound impact on how solutes are transported through the porous medium, influencing how effective large-scale transport should be modeled. Here we simulate, using high-resolution numerical models, flow and transport through an idealized porous medium for flow conditions over a range of Reynolds numbers, including steady and unsteady flows. For all these conditions we propose and test three upscaled models for transport—an advection dispersion equation, an uncorrelated spatial model (USM) and a spatial Markov model (SMM). The USM and SMM fall into the wider and more general family of continuous time random walk models. We test these models by their ability to reproduce pre-asymptotic and asymptotic plume second centered moments and breakthrough curves. We demonstrate that for steady flows where inertial effects are strong, the spatial Markov model outperforms the other two, faithfully capturing many of the non-Fickian features of transport, while for unsteady flows the uncorrelated spatial model performs best, due to the fact that unsteadiness in the flow field dampens the role of correlation on large scale transport. We conclude that correlation must be accounted for to properly upscale transport in steady flows, while it can be neglected in unsteady flows.

Keywords Dispersion · Random walk · Inertia · Nonlocal

✉ Nicole Sund
nsund@nd.edu

[1] Department of Civil and Environmental Engineering and Earth Sciences, University of Notre Dame, Notre Dame, IN 46556, USA

[2] The Institute for Computational Engineering and Sciences, The University of Texas at Austin, Austin, TX 78712, USA

Published online: 16 June 2015

1 Introduction

While much research on flow and transport in porous media has focused on low Reynolds number regimes, there are many examples where higher Reynolds number flows are important. Common examples can include flow through fractured systems (Cardenas et al. 2009), CO_2 sequestration in geologic media (Bachu 2003; Vilarrasa et al. 2010), flow through industrial porous reactors (Freund et al. 2003), flow in close proximity of wells (Wen et al. 2006) and flow through wetlands where plants act as the solid phase of an effective porous medium (Nepf et al. 1997). At low Reynolds numbers, $\mathrm{Re} << 1$, flow at the pore scale can be described by Stokes flow equations and upscaled effectively to Darcy's law. As Reynolds numbers become sufficiently large for inertial effects to play a role (i.e., $\mathrm{Re} = O(1)$), this no longer holds and alternative effective models, such as Darcy–Forchheimer, are needed (Chaudhary et al. 2011, 2013). At the pore scale the streamline structure of the flow changes and features such as recirculation zones can emerge. As Reynolds numbers become even larger, the flow can become unsteady, and at even higher values, the flow becomes turbulent.

In addition to influencing the flow field, inertial effects, which become important as the Reynolds number becomes greater than one, can have an impact on transport (Bouquain et al. 2012; Richmond et al. 2013; Cardenas 2008; Wood 2007). In fact, soluble contaminants in water most commonly have Peclet numbers that are O(1000 × Reynolds number), meaning that advective effects can play an important role on transport, even when they do not on flow. As the Reynolds number becomes larger and larger, the flow can become unsteady and even turbulent, which is known to affect mass transfer by decreasing dispersive spreading, in such systems (White and Nepf 2003; Richmond et al. 2013). This potentially poses a significant challenge in developing upscaled models for transport in flows through porous media at large Reynolds numbers.

The pioneering works of Taylor (1953) and Aris (1956) show that transport in a tube can, at asymptotic times, be described by an effective one-dimensional advection dispersion equation (ADE), where an effective constant dispersion coefficient quantifies the growth of the second centered spatial moment (variance) of the plume. These ideas were later generalized to more complex flow configurations using a variety of methods including empirical correlations (Delgado 2007), homogenization (Hornung 1997), the method of volume averaging (Whitaker 1998) and the method of moments (Brenner 1980). Such models are ubiquitously applied in transport studies through porous media, and while incredibly powerful, a key limitation of such approaches is that they are, strictly speaking, only valid at asymptotic times, meaning after times when the solute has had time to sample the full distribution of velocities. This is quantified by timescale $\tau_D = l^2/D$, where l is a characteristic length scale of the system in question and D is the diffusion coefficient of the solute. Depending on the specific application this timescale may be prohibitively long to make predictions over time and length scales of interest.

At pre-asymptotic times, or times less than τ_D, it is typically observed that the second centered moment grows superdiffusively in time (faster than linear in time), an observation that cannot be reproduced by an effective advection dispersion equation with constant dispersion coefficient. To rectify this, many of the above-mentioned approaches have been generalized to include transient dispersion coefficients that change in time and can successfully match the superdiffusive growth of a plume's second centered moment (Dentz et al. 2000). However, matching the growth of the second centered moment of a plume is not a sufficient condition for proper upscaling of solute transport as it may yield inaccurate predictions of downstream arrival times and spatial distributions of mean concentration (Dentz and Bolster 2010; Fitts 1996).

Heterogeneity in the flow field due to the presence of the solid phases gives rise to features such as no-slip boundaries, dead-end pores, recirculation zones and preferential flow pathways. These all result in a broad distribution of velocities and associated time scales, a feature that is difficult to include properly in conventional models at pre-asymptotic times. However, a rich class of nonlocal models has emerged that are able to capture observed non-Fickian behavior. These include multi-rate mass transfer models (Haggerty and Gorelick 1995), fractional advection dispersion equation (Benson et al. 2000; Cushman and Ginn 2000) and continuous time random walk models (CTRW) (Montroll and Weiss 1965; Scher and Lax 1973; Berkowitz et al. 2006; Edery et al. 2014). With appropriate implementation these models can naturally transit from pre-asymptotic superdiffusive to asymptotic diffusive behavior (Dentz et al. 2004; Meerschaert et al. 2008). While conceptually distinct, these models can be related to one another (e.g., Margolin et al. 2003; Neuman and Tartakovsky 2009; Berkowitz et al. 2002; Schumer et al. 2003; Dentz and Berkowitz 2003).

To account for cases in which correlation effects are significant, Le Borgne et al. (2008b) proposed a spatial Markov model that allows for the inclusion of correlation effects. It should be noted that this model is a specific implementation of and falls into the family of more general CTRW models. This model has been successfully applied to transport through heterogeneous porous media (Le Borgne et al. 2008a, b), a fracture network (Kang et al. 2011), low Reynolds number pore scale transport through a porous medium (Le Borgne et al. 2011; de Anna et al. 2013) and transport through a wavy channel, where inertial effects were large, but flow remained steady ($1 < \mathrm{Re} < 100$) (Bolster et al. 2014). In particular Bolster et al. (2014) showed that correlation effects must be included when $\mathrm{Pe} > O(100)$. Below this critical Peclet number, an uncorrelated spatial model worked well, but above it only the spatial Markov model was successfully able to upscale transport. Given that for many solutes of interest in water, $\mathrm{Pe} = O(1000\mathrm{Re})$, once inertial effects are important for flow (i.e., $\mathrm{Re} \geq O(1)$), it may be critical to include correlation in effective transport models. However, once the Reynolds number becomes sufficiently large that the flow becomes unsteady, the unsteadiness in the flow may act in such a way as to reduce correlation effects, as suggested by observations that unsteady and turbulent flows through porous media may actually reduce effective solute dispersion (White and Nepf 2003; Nepf et al. 1997; Richmond et al. 2013).

In this work, we explore the ability of the spatial Markov model, the uncorrelated spatial model and the ADE, with both constant and transient dispersion coefficients, to predict transport through an idealized porous medium with Reynolds numbers ranging from 15 to 280. This range of Reynolds numbers spans the steady inertial flow regime and the unsteady flow regime. We begin by describing the high-resolution microscale flow (Sect. 2) and transport (Sect. 3) simulations. The microscale transport simulations are used as benchmarks for comparison to the upscaled models as well as to parameterize the upscaled models. We then describe the upscaled models (Sect. 4) and how they were implemented. We finally discuss results (Sect. 5) and concluding remarks (Sect. 6).

2 Microscale Flow

We consider flow through a two-dimensional periodic domain as depicted in Fig. 1. The domain is rectangular and of size $L \times L$ with circular solid obstacles of diameter $L/2$ included. To obtain the flow field we solve the full Navier–Stokes equations with a dynamic Smagorinsky turbulence model,

Fig. 1 Unit cell

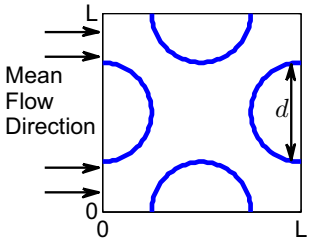

$$\begin{aligned} \frac{\partial \mathbf{u}(\mathbf{x},t)}{\partial t} + \Big(\mathbf{u}(\mathbf{x},t)\cdot\nabla\Big)\mathbf{u}(\mathbf{x},t) &= -\frac{\nabla P(\mathbf{x},t)}{\rho} + (\nu+\nu_t)\nabla^2\mathbf{u}(\mathbf{x},t) + \mathbf{f} \\ \nabla\cdot\mathbf{u}(\mathbf{x},t) &= 0, \end{aligned} \tag{1}$$

where $\mathbf{u}(\mathbf{x},t)$ is the fluid velocity, $P(\mathbf{x},t)$ is the pressure field, ρ is the density of the fluid, ν is the kinematic viscosity of the fluid, ν_t is the turbulent viscosity, and $\mathbf{f} = [f_x, 0]^T$ is a constant horizontal body force. The turbulent viscosity is defined using a dynamic Smagorinsky model,

$$\nu_t = (C_\mathrm{s}\Delta_\mathrm{g})^2\sqrt{2S_{ij}S_{ij}}, \tag{2}$$

where Δ_g is the grid size, C_s is the Smagorinsky coefficient, and $S_{ij} = \frac{1}{2}\left(\frac{\partial u_i}{\partial x_j} + \frac{\partial u_j}{\partial x_i}\right)$ is the strain-rate tensor. C_s is calculated on each grid cell at each time step according to a simplification of the dynamic model from Germano et al. (1991) developed by Voke (1996) and Meneveau and Lund (1997). This turbulence closure model is designed to model turbulence from laminar ($C_s = 0$), transitional and fully turbulent flow and is discussed thoroughly by Mattis et al. (2012).

We use a no-slip boundary condition on the obstacle boundary (Γ_o) and periodic boundary conditions on the edges of the domain

$$\begin{aligned} \mathbf{u}(\mathbf{x},t) &= 0 \text{ on } \Gamma_o \\ \mathbf{u}(x=0,y,t) &= \mathbf{u}(x=L,y,t) \\ \mathbf{u}(x,y=0,t) &= \mathbf{u}(x,y=L,t) \\ P(x,y=0,t) &= P(x,y=L,t) \\ P(x=0,y,t) &= P(x=L,y,t). \end{aligned} \tag{3}$$

We impose a constant horizontal forcing term f_x over the domain to drive the flow. The equations are solved on an unstructured mesh using triangular elements with linear basis functions. We use a locally conservative, stabilized finite element method outlined by Kees et al. (2009) using the Proteus Computational Methods and Simulation Toolkit (http://proteus.asace.army.mil). The backward Euler implicit time integration method is used for time stepping. Details of the numerical method are available in Mattis et al. (2012). We consider several cases with a range of Reynolds numbers from 15 to 280. Here we define the Reynolds number as

$$\mathrm{Re} = \frac{\overline{u}d}{\nu}, \tag{4}$$

where $\overline{u}$ is the mean flow velocity, d is the diameter of the obstacles, and ν is the kinematic viscosity. The Reynolds number quantifies the relative influence of advective (inertial) effects against viscous effects in the flow.

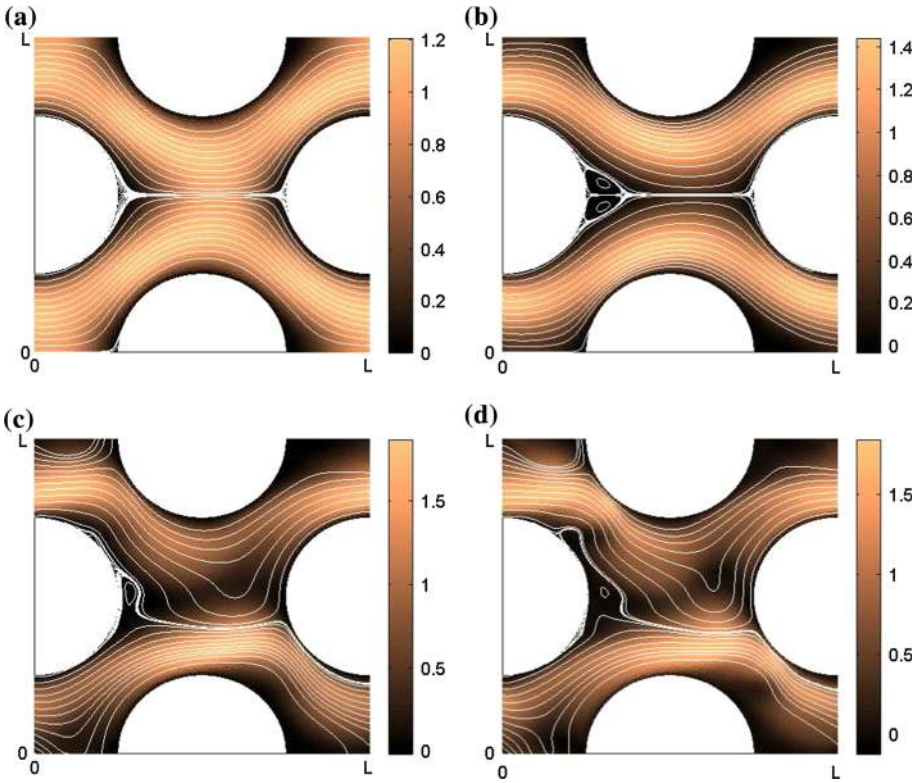

Fig. 2 Velocity field snapshots for **a** Re = 15, **b** Re = 80, **c** Re = 145, and **d** Re = 280. The *white lines* are streamlines, and the *color* indicates the velocity in the x-direction. For the steady flows (**a**) and (**b**) the streamlines are the same at all times, while for the unsteady flows (**c**) and (**d**) they change in time and these figures depict an instantaneous snapshot at one particular time

The model was run with different forcing terms to obtain velocity fields for different Reynolds numbers. Figure 2 shows snapshots in time of velocity fields for various Reynolds numbers along with streamlines. For the lowest Reynolds number (a), the velocity field is symmetric with respect to the line $y = L/2$ and we can just begin to see the formation of recirculation zones behind the obstacles. As the Reynolds number increases to 80 (b), the velocity field is still symmetric, but the recirculation zones are much larger and clearly visible. For higher Reynolds numbers (c) and (d), the symmetry is gone and the flow field is unsteady, as the recirculation zones continually shed from the obstacles. Also note that the range of velocities increases with Reynolds number. Increasing inertial effects, causing the change in structure of the streamlines and the broadening of velocity scales are likely to lead to greater longitudinal dispersion of solutes as well as greater non-Fickian behavior. Additionally, the eventual transition to unsteady flow is likely to influence transport in a significant manner.

3 Microscale Transport

We consider transport at the pore scale as governed by the advection–diffusion equation,

$$\frac{\partial C(\mathbf{x},t)}{\partial t} + \mathbf{u}(\mathbf{x},t)\cdot\nabla C(\mathbf{x},t) = D\nabla^2 C(\mathbf{x},t) \tag{5}$$

where C is the concentration of a conservative solute, $\mathbf{u}(\mathbf{x}, t)$ is the velocity given by the pore scale flow simulations, and D is a constant representing molecular diffusion. We use a no-flux boundary condition on the obstacles (Γ_o) and periodic boundaries at the edges of the domain. We use a flux-weighted delta pulse initial condition distributed across the entire vertical length of the inflow boundary.

$$\begin{aligned} \frac{\partial C(\mathbf{x}, t)}{\partial n} &= 0 \text{ on } \Gamma_o \\ C(x = 0, y, t) &= C(x = L, y, t) \\ C(x, y = 0, t) &= C(x, y = L, t) \\ C(\mathbf{x}, 0) &\propto \mathbf{u}(\mathbf{x}, 0)\delta(x). \end{aligned} \tag{6}$$

We solve this equation using a classical random walk method (Risken 1984). The solute plume is discretized into a large, but finite number (N) of particles. Each particle's motion is then governed by the Langevin equation

$$\begin{aligned} \mathbf{x}_{n+1} &= \mathbf{x}_n + \mathbf{u}\Delta t + \sqrt{2D\Delta t}\xi_n \\ t_{n+1} &= t_n + \Delta t. \end{aligned} \tag{7}$$

where $\xi_n \sim N(\mathbf{0}, \mathbf{I}_2)$ is a two-dimensional vector consisting of independent random Gaussian variables with zero mean and unit variance and $\mathbf{u}$ is the velocity from the pore scale flow simulation, which is calculated by finding which element the particle is located within and then interpolating the velocity exactly using the nodal basis functions. To obey the no-flux boundary condition, the obstacle boundaries are modeled as elastic reflection boundaries, that is, if $\mathbf{x}_{n+1}$ lies across an obstacle boundary, then its reflected position is $\mathbf{x}^r_{n+1} = 2(\mathbf{x}_n + \text{proj}_{\Gamma_o}(\mathbf{x}_{n+1} - \mathbf{x}_n)) - \mathbf{x}_{n+1}$ where proj_{Γ_o} is the projection onto the obstacle boundary Γ_o.

For transport the dimensionless number of interest is the Peclet number,

$$\text{Pe} = \frac{\overline{u}d}{D}, \tag{8}$$

which is similar in structure to the Reynolds number and quantifies the relative influence of advective effects to diffusive effects on transport. Note that we can define the Schmidt number as the ratio of Peclet to Reynolds numbers,

$$\text{Sc} = \frac{\text{Pe}}{\text{Re}} = \frac{\nu}{D}, \tag{9}$$

which is also the ratio of fluid viscosity to solute diffusivity. The diffusion coefficient, D, is chosen so that in all simulations the Schmidt number is 500, which is characteristic of many solutes in water (Mills 1999). Since we fix the Schmidt number, for the chosen range of Reynolds numbers, the Peclet number ranges from 7.5×10^3 to 1.4×10^5. A sample snapshot of the spatial distribution of particles at a fixed time is shown in Fig. 3 for four of the Reynolds numbers simulated. For the steady flows (a) and (b), we can visually see the effect of large Peclet number, where particles closely follow the streamlines they start on, with a small amount of dispersion. On the other hand the particles in unsteady flows (c) and (d) show no memory of their initial condition, appearing more mixed across the domain. We also see, though, that particles are being caught in the shedding vortices and swept downstream in clusters.

In order to assess the ability of the effective upscaled models, presented in the following section, to replicate the behavior of the microscale simulations we will focus on measuring and comparing two common transport metrics:

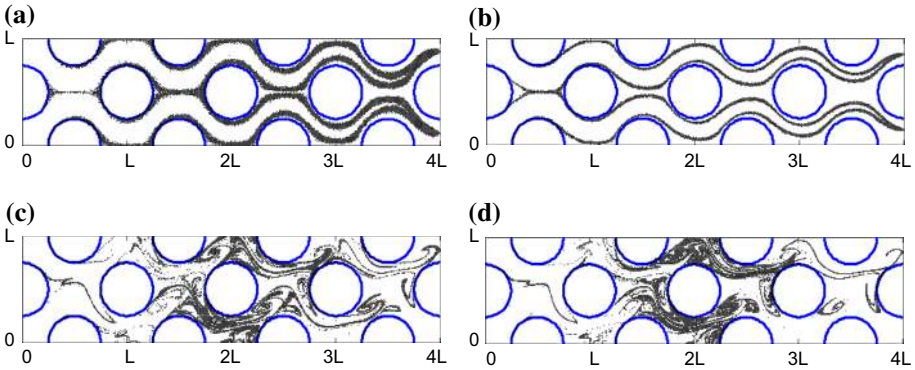

Fig. 3 Spatial distribution of particles at the moment when a single particle crosses the unit cell four times for different Reynolds numbers. Steady flows: **a** Re $= 15$, Pe $= 7.5 \times 10^3$ and **b** Re $= 80$, Pe $= 4.0 \times 10^4$. Unsteady flows: **c** Re $= 145$, Pe $= 7.3 \times 10^4$ and **d** Re $= 280$, Pe $= 1.4 \times 10^5$

- *Second centered moment of the plume* The second centered moment of a plume is a common measure of the rate of spreading around the center of mass. It is defined as

$$\sigma^2(t) = \int_{-\infty}^{\infty} x^2 C(\mathbf{x}, t)\mathrm{d}x - \left(\int_{-\infty}^{\infty} x C(\mathbf{x}, t)\mathrm{d}x \right)^2, \tag{10}$$

  or in terms of particle locations

$$\sigma^2(t) = \frac{1}{N} \sum_{i=1}^{N} x_i(t)^2 - \left(\frac{1}{N} \sum_{i=1}^{N} x_i(t) \right)^2. \tag{11}$$

- *Breakthrough curves* Breakthrough curves are a measure of the concentration arriving at a fixed downstream location over time. In this work we will focus on breakthrough curves at distances of $10L$, $100L$ and $1000L$ downstream from the injection location.

As highlighted in the work of Dentz and Bolster (2010) it is necessary to check at least both of these metrics for model validation, as it is possible for a model to adequately match one of the metrics, while failing to capture the other. This will be demonstrated for some of the upscaled models in Sect. 4. Successfully matching both of these metrics suggests greater strength of the upscaled model to capture the spatio-temporal dynamics that evolve due to microscale physics.

4 Upscaled Models

Using the microscale flow and transport simulations, we parameterized three upscaled models: the conventional ADE model (4.1), an uncorrelated spatial model (4.2) and the spatial Markov model (4.3). Each model can be run a number of ways, so here we compare some of the options of each model in order to ultimately select models to be used in an inter-model comparison shown in Sect. 5. Throughout subsequent sections, the following notation will be used:

$$
\begin{aligned}
f_*(t) &= \text{distribution of } * \text{ as measured in the microscale simulations,} \\
\tau_i &= \text{time it took a microscale particle to travel from } x = (i-1)L \text{ to } x = iL, \\
S_\xi &= \sum_{i=1}^{\xi} \tau_i = \text{time it took a particle to travel from } x = 0 \text{ to } x = \xi L.
\end{aligned} \tag{12}
$$

4.1 ADE

The first model that we consider is an upscaled one-dimensional ADE, described by

$$
\frac{\partial C}{\partial t} + \overline{u}\frac{\partial C}{\partial x} = D_L(t)\frac{\partial^2 C}{\partial x^2}. \tag{13}
$$

Note this equation is similar in structure to (5), but is only in 1-d and does not resolve the flow field, but rather aims to capture subscale variations through an effective longitudinal dispersion coefficient, $D_L(t)$. Two variants of this model are considered, one where $D_L(t)$ is allowed to evolve in time, and another where D_L is constant and given by the asymptotic Taylor dispersion coefficient. Specifically

$$
D_L(t) = \frac{1}{2}\frac{\mathrm{d}\sigma^2(t)}{\mathrm{d}t}, \tag{14}
$$

where $\sigma^2(t)$ is the variance of the microscale particle positions. In this case we directly use $\sigma^2(t)$ as measured from the microscale simulations, rather than developing a model for it using an upscaling approach, such as volume averaging (for example Richmond et al. 2013). Our goal here is not to develop a model for the transient effective dispersion coefficient, but rather to show the results that would emerge from implementing one. The asymptotic value of D_L comes from taking the late time limit of (14). The models are called the pre-asymptotic and asymptotic ADE models, respectively.

Figure 4 compares the asymptotic and pre-asymptotic ADE models' predictions of $\sigma^2(t)$ to the actual microscale simulation data. By design, the pre-asymptotic ADE is a perfect match, since this is the data used to parameterize the model. The asymptotic ADE, on the other hand,

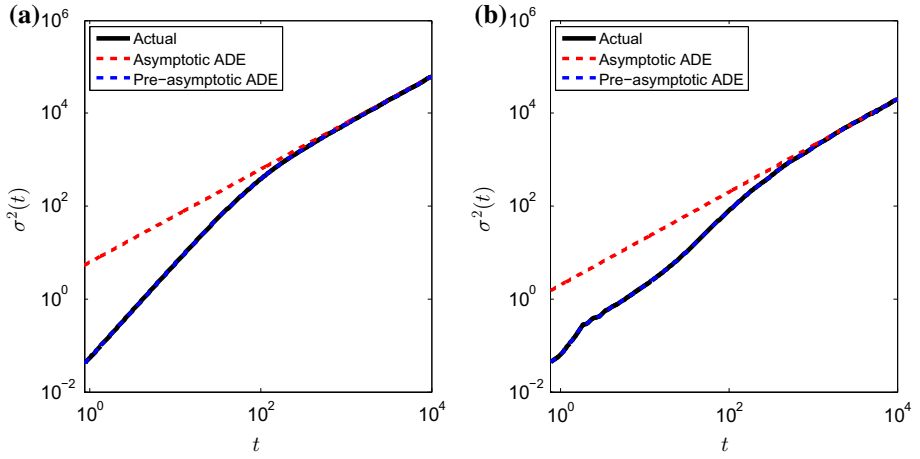

Fig. 4 ADE predictions using asymptotic and pre-asymptotic dispersion coefficients of $\sigma^2(t)$ for **a** Re = 15 (steady flow) and **b** Re = 280 (unsteady flow)

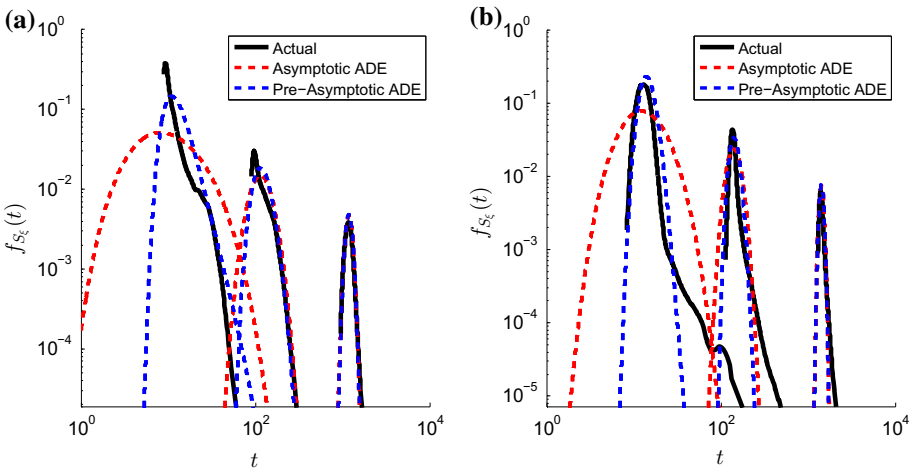

Fig. 5 ADE predictions using asymptotic and pre-asymptotic dispersion coefficients of breakthrough curves, $f_{S_\xi}(t)$, at $x = \xi L$ for $\xi = 10$, 100, and 1000 for **a** Re $= 15$ (steady flow) and **b** Re $= 280$ (unsteady flow)

is only able to match $\sigma^2(t)$ at late times and significantly overpredicts spreading at early times. Figure 5 compares breakthrough curves of the asymptotic and pre-asymptotic ADE models to the actual microscale simulation data at three downstream locations, $x = 10L$, $x = 100L$ and $x = 1000L$. The pre-asymptotic ADE again performs better, as the breakthrough curves of the asymptotic ADE are severely over spread. However, other than at late times, this is hardly a good match, particularly for the steady flow field case. These results highlight and verify that having a model matching the second centered moment of a plume does not guarantee that the spatio-temporal dynamics of the plume are accurately described (Fitts 1996; Dentz and Bolster 2010).

4.2 Uncorrelated Spatial Model

From the microscale model described in Sect. 3, we measure the amount of time it takes each particle to traverse the first unit cell (τ_1) and also how long it takes the same particle to traverse the second unit cell (τ_2). This allows us to calculate the joint distribution for τ_1 and τ_2, $f_{\tau_1 \& \tau_2}(t)$, which is all of the information we need for both of the spatial models. For the spatial models we discretize the solute plume into N particles of equal mass. Then each particle at step n is moved according to:

$$\begin{aligned} x_{n+1} &= x_n + \xi_* L \\ t_{n+1} &= t_n + \Delta t_n \end{aligned} \tag{15}$$

where ξ_* is a natural number and the Δt_n's are samples from a chosen distribution $f(\Delta t)$. In the uncorrelated spatial model,

$$f(\Delta t) = f_{S_{\xi_*}}(t), \tag{16}$$

where $f_{S_{\xi_*}}(t)$ is the distribution of travel times from $x = 0$ to $x = \xi_* L$ obtained from the microscale simulations.

The uncorrelated spatial model is equivalent to a very specific form of more general CTRW models, that is, one with fixed spatial increment and independent identically distributed time

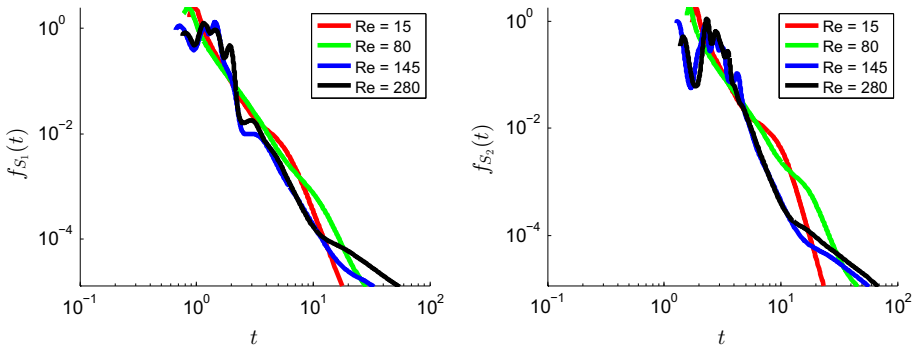

Fig. 6 S_ξ distributions, $f_{S_\xi}(t)$, for various Reynolds numbers with (*left*) $\xi = 1$ and (*right*) $\xi = 2$

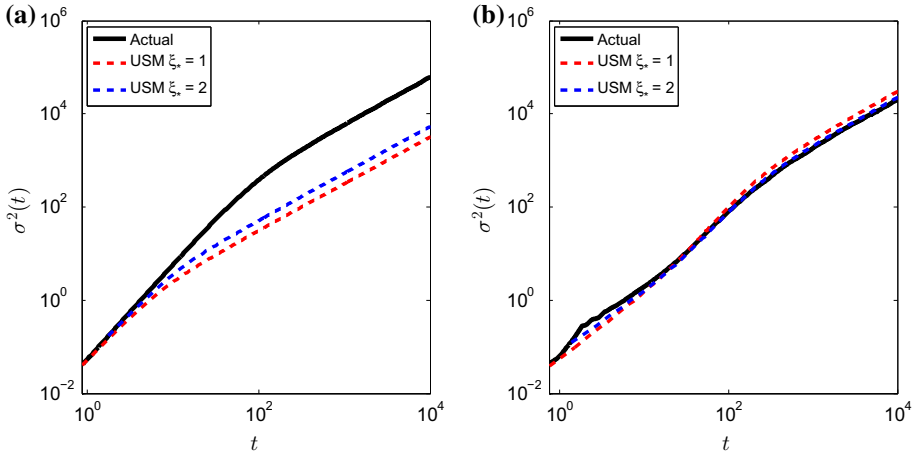

Fig. 7 Uncorrelated spatial model predictions using $\xi_* = 1, 2$ of $\sigma^2(t)$ for **a** Re $= 15$ (steady flow) and **b** Re $= 280$ (unsteady flow)

increments. Figure 6 shows $f_{S_1}(t)$ and $f_{S_2}(t)$ for various Reynolds numbers. Note the sharp peaks and non-monotonically decreasing tails, which are consistent with observations from Bolster et al. (2014) and indicative of the fact that a Fickian ADE model, such as those presented in the previous subsection, will not be able to capture early time dynamics well. The distribution $f_{S_2}(t)$ is wider and smoother than $f_{S_1}(t)$ but still displays non-monotonic behavior, a feature an ADE model cannot capture.

Since for the spatial Markov model, described in detail below, we will use information about the travel times across both the first and second periodic element, we will also consider both options for the uncorrelated spatial model, in order to create a fair ultimate inter-model comparison. Figure 7 shows the uncorrelated spatial models' predictions of the second centered moment of the solute plume, $\sigma^2(t)$, and compares them to the actual data from the microscale simulations. Figure 8 shows the models' predictions of breakthrough curves, $f_{S_\xi}(t)$ for $\xi = 10, 100$, and 1000. Although both models yield relatively similar results, it comes as no surprise that using a larger ξ_* gives slightly better results. As ξ increases, correlation effects become less important as will be discussed in greater detail below. In fact Bolster et al. (2014) showed that if ξ_* is chosen large enough, an uncorrelated spatial model

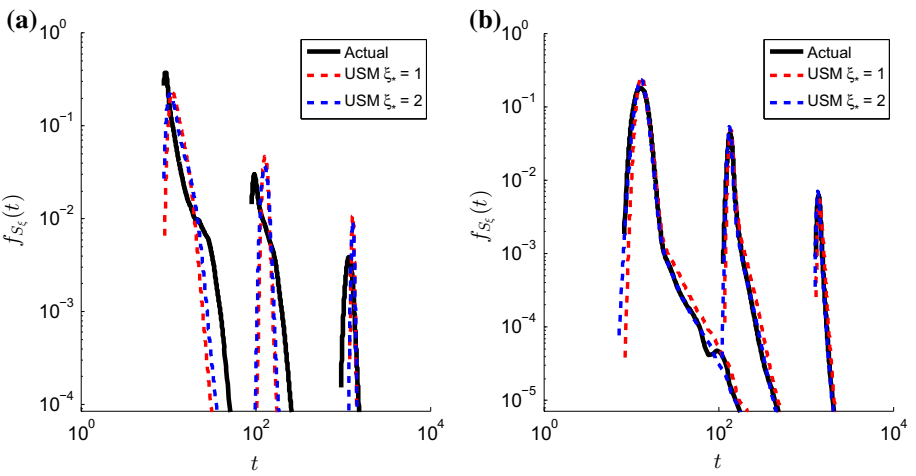

Fig. 8 Uncorrelated spatial model predictions using $\xi_* = 1, 2$ of breakthrough curves, $f_{S_\xi}(t)$, at $x = \xi L$ for $\xi = 10$, 100, and 1000 for **a** Re $= 15$ (steady flow) and **b** Re $= 280$ (unsteady flow)

should perform well. It is only at this asymptotic length scale that the uncorrelated spatial model is truly valid. Choosing ξ_* with $\xi_* L$ smaller than the asymptotic length scale creates a tendency for the uncorrelated spatial model to underpredict the spreading of the solute plume as seen for the steady flow case in Fig. 7a, where the models underpredict $\sigma^2(t)$ by more than an order of magnitude and are unable to capture the shape of the breakthrough curves (Fig. 8). However, for the unsteady flow, the uncorrelated spatial model appears to capture the evolution of the second centered moment and the breakthrough curves well. The reason for this will be discussed in greater detail below.

4.3 Spatial Markov model

In the spatial Markov model we set $\xi_* = 1$ in Eq. 15 and choose Δt from

$$f(\Delta t) = \begin{cases} f_{\tau_1}(t) & \text{for } n = 1 \\ f(\Delta t_n | \Delta t_{n-1}) & \text{for } n = 2, \ldots \end{cases} \tag{17}$$

where we approximate $f(\Delta t_n | \Delta t_{n-1})$ by discretizing $f_{\tau_1}(t)$ into β travel time classes, or bins. If $\beta = 1$, then the model reduces to the uncorrelated spatial model. If $\beta > 1$, the spatial Markov model is equivalent to another specific form of more general CTRW models, that is, one with fixed spatial increment and correlated time increments. Using the joint distribution $f_{\tau_1 \& \tau_2}(t)$, for each microscale particle we assign an initial class (given by τ_1) and its new class (given by τ_2). From these statistics we arrive at the discrete joint distribution $P(\tau_1 \in \text{bin } i \& \tau_2 \in \text{bin } j)$. From this we can get $P(\tau_2 \in \text{bin } j | \tau_1 \in \text{bin } i)$ given by

$$P(\tau_2 \in \text{bin } j | \tau_1 \in \text{bin } i) = \frac{P(\tau_1 \in \text{bin } i \& \tau_2 \in \text{bin } j)}{P(\tau_1 \in \text{bin } i)}. \tag{18}$$

Further details of this procedure are available in Le Borgne et al. (2008a, 2011) and Bolster et al. (2014). We then model the steps of the spatial Markov model as a spatially homogeneous Markov process with β discrete states, which can be described with a transition probability matrix, T_{ji}, defined as,

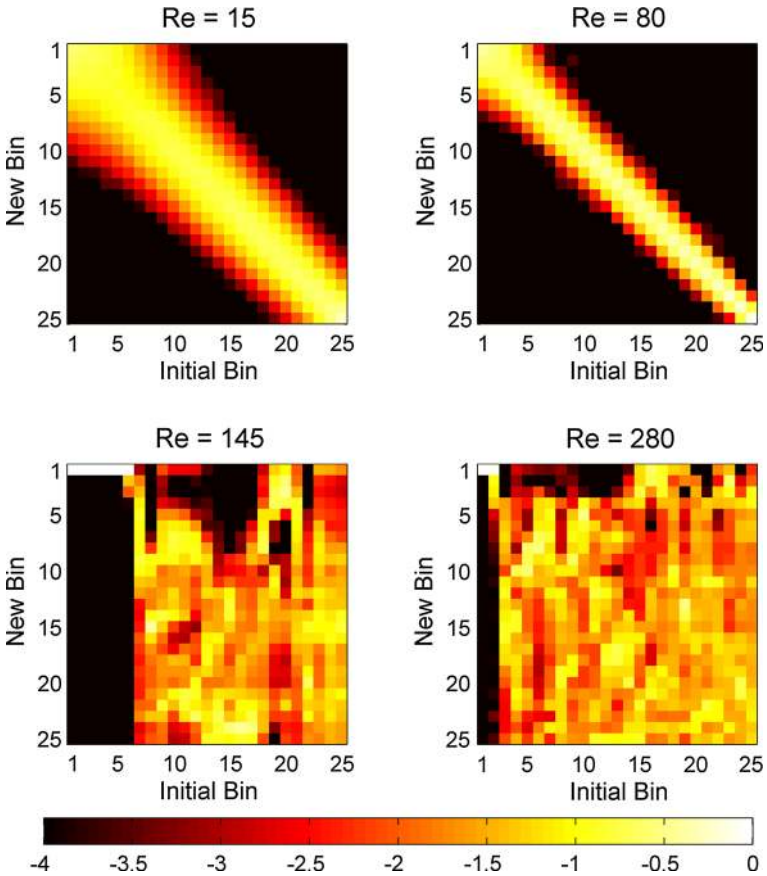

Fig. 9 Log of transition matrices, $\log_{10}(T_{ji})$, for (*top*) steady flow and (*bottom*) unsteady flow using $\beta = 25$ bins

$$T_{ji} = P(\tau_{n+1} \in \text{bin } j | \tau_n \in \text{bin } i) = P(\tau_2 \in \text{bin } j | \tau_1 \in \text{bin } i). \tag{19}$$

This assumes that between any two adjacent jumps, the correlation structure is the same. In steady velocity fields this assumption should be satisfied, as the streamline structure is the same in each unit cell (Bolster et al. 2014). In the unsteady velocity fields, this need not be true, but despite this we test the model anyway. Note that, as currently implemented, the SMM has the limitation that it requires full information of the velocity field to measure transition time distributions and transition matrices.

Figure 9 shows the transition matrices for steady and unsteady flows with 25 bins. When the flow is steady, the transition matrix is a diagonally dominant banded matrix with a bandwidth that decreases as the Peclet number increases. This is consistent with previous studies Le Borgne et al. (2008a, 2011), Bolster et al. (2014) and de Anna et al. (2013). This is due to increased transition time correlation with increasing Peclet number. Physically this is because particles with low diffusion tend to stay on the same or similar streamlines as they pass through successive periodic elements. For the steady fields, there is stronger correlation of the particles in the higher bin numbers, which correspond to the longest times, or the lowest velocities.

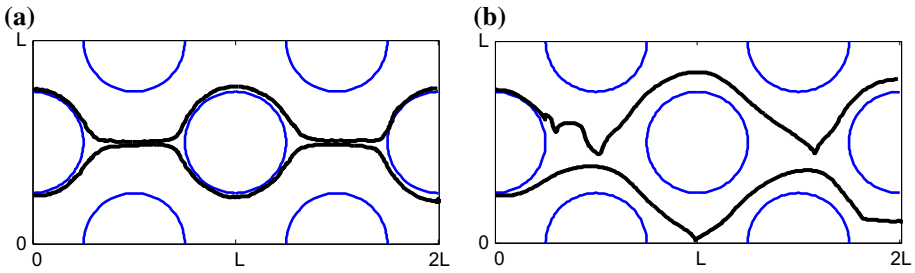

Fig. 10 Sample particle paths for **a** steady and **b** unsteady velocity fields. Note that in the steady field the particles follow an almost identical path over the first and second periodic element, while the paths are quite different for the unsteady flow

On the other hand, for the unsteady flows, there appears to be little definable structure to the transition matrices as measured, that is, from a pulse initial condition at the inlet of the domain, an issue that will be discussed in further detail below. This is due to the fact that in unsteady flows, a particle's travel time depends not only on which streamline it is on, but also on the changing structure of that streamline over the measured time period. To highlight this, Fig. 10 depicts the path line of two particles in both a steady and unsteady flow, clearly showing that the path followed over the first and second periodic element is almost identical for the low Reynolds number case, while the paths are quite distinct in the larger Reynolds number flow. That being said there is one feature of the transition matrices that stands out. There is a strong correlation of the particles in the lower bin numbers, which correspond to the shortest transit times, or highest velocities.

While for steady flows it is known that increasing the number of bins β in the transition matrix will yield improved results given a sufficient number of particles (Le Borgne et al. 2011), this may not hold true for the unsteady flows due to the unstructured nature of the perhaps insufficiently resolved transition matrix (again see discussion below for further details). Due to the fact that the high-velocity bins in the unsteady flows appear to show an important structure, we will explore two values of β: $\beta = 2$ and 25. $\beta = 2$ is chosen to capture the high-velocity correlation effects in the unsteady flow and can be thought of as a model that distinguishes between highly mobile and highly immobile particles, similar to a multi-rate mass transfer model (Haggerty and Gorelick 1995). $\beta = 25$ is chosen as it adequately resolves the correlation for the steady flow cases (i.e., doubling the number of bins to 50 does not improve the model predictions). The transition matrices for $\beta = 2$ are shown in Fig. 11, which, in all cases, show a diagonal dominance.

Figure 12 compares the spatial Markov model's predictions of the second centered moment of the solute plume using $\beta = 2, 25$ to the actual data from the microscale simulations. Figure 13 compares the same models' predictions of breakthrough curves, $f_{S_\xi}(t)$ for $\xi = 10$, 100, and 1000 to the actual data. For the steady flow the model with the larger number of bins appears to adequately capture behavior of both the second centered moment and the breakthrough curves. On the other hand, for the unsteady flow the model with the lower number of bins outperforms the larger bin model. In fact the larger bin model completely fails to capture the evolution of the second centered moment at late times and yields unphysical results, suggesting that it is imposing an artificial and inaccurate correlation structure. This is reflected in the breakthrough curves where the plume seems to be arriving much faster and is much less disperse than the observations. Based on these results, for inter-model comparison in the following section, we will use $\beta = 2$ for unsteady flows and $\beta = 25$ for steady flows for the spatial Markov model.

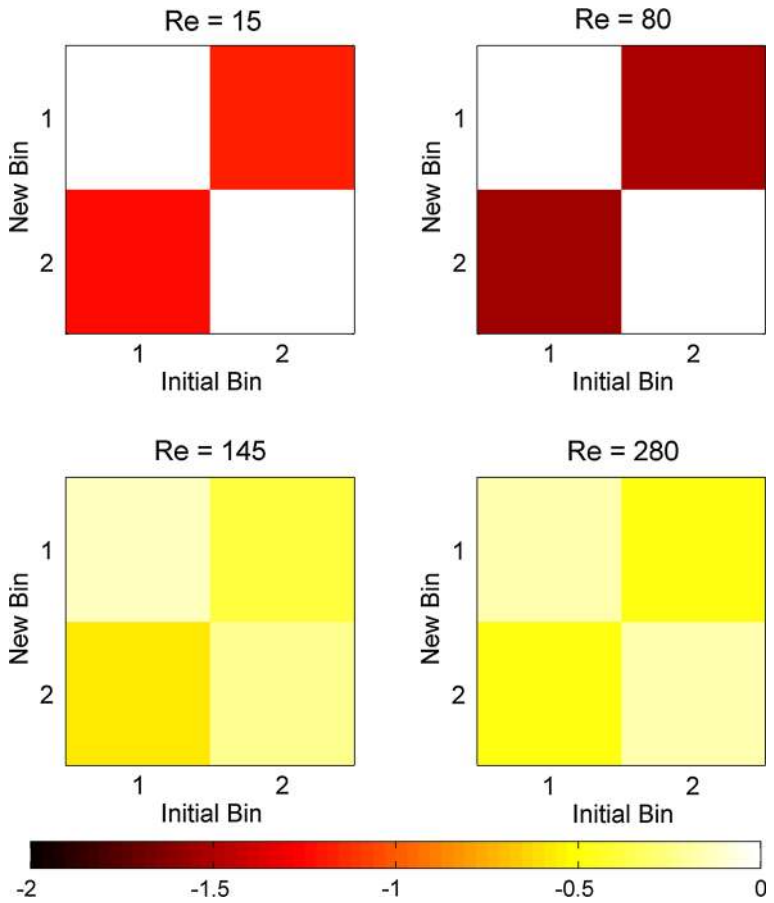

Fig. 11 Log of transition matrices, $\log_{10}(T_{ji})$, for (*top*) steady flow and (*bottom*) unsteady flow using $\beta = 2$ bins

The so-called artificial correlation that we mention above for the unsteady flows and $\beta = 25$ case appears to be an artifact of how the correlation matrix is measured. Specifically, as in previous studies, the correlation matrix is measured using a pulse initial condition and then tracking travel times across two elements. For a steady flow this appears to be a reasonable manner in which to measure the transition matrix, given how well it works here and in previous studies. However, for unsteady flows, it may not be adequate. Due the fact that the flow field is changing in time, by tracking a pulse initial condition one is only measuring correlations associated with the field for that particular initial condition, which may not reflect the full array of dynamics in the system. Indeed if we choose a different time at which to inject the pulse, we measure quite a different transition matrix from the one presented in Fig. 9. When, instead of measuring the transition time distribution from a single pulse, we measure the transition matrix from various pulses, each injected at different times, the transition matrix becomes more uniform. As this number of pulses increases the transition matrix homogenizes more and more, explaining why the USM appears to work so well as it can be thought of as corresponding to a transition matrix that is completely uniform (i.e., all particles have equal access to any other bin regardless of their previous transition time).

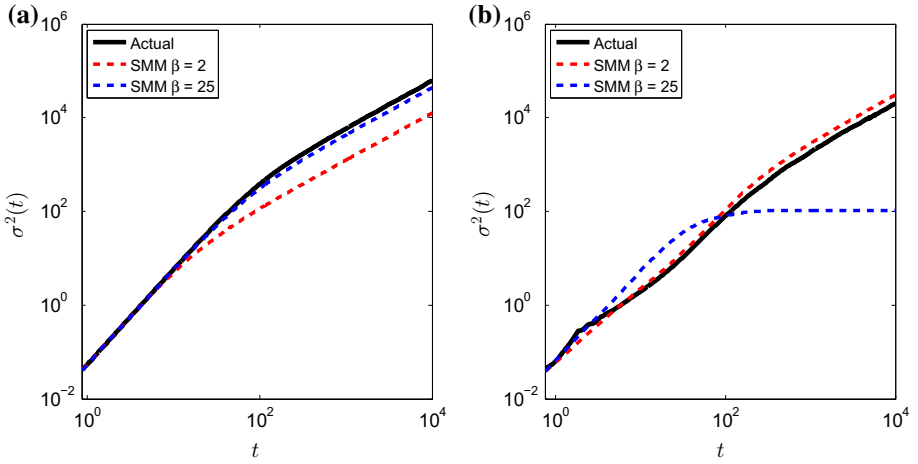

Fig. 12 Spatial Markov model predictions using $\beta = 2, 25$ of $\sigma^2(t)$ for **a** Re $= 15$ (steady flow) and **b** Re $= 280$ (unsteady flow)

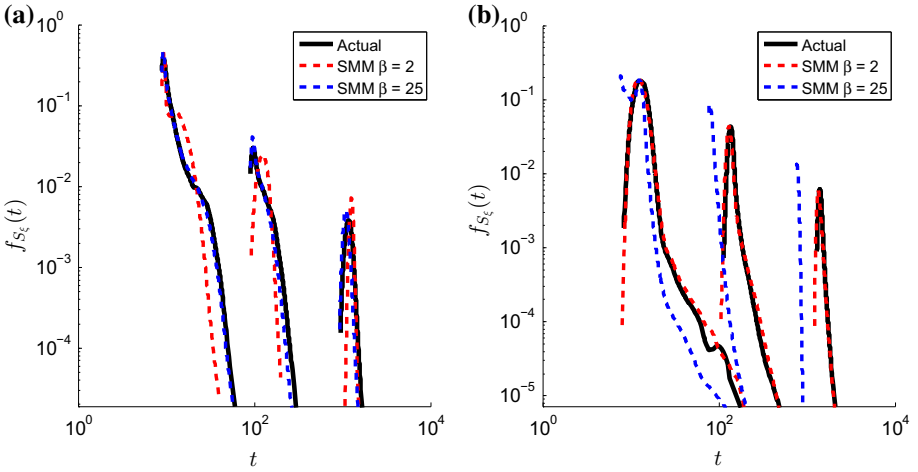

Fig. 13 Spatial Markov model predictions using $\beta = 2, 25$ of breakthrough curves, $f_{S_\xi}(t)$, at $x = \xi L$ for $\xi = 10, 100$, and 1000 for **a** Re $= 15$ (steady flow) and **b** Re $= 280$ (unsteady flow)

This suggests that the traditional manner of measuring the transition matrix, from a single pulse, is not adequate and presents a potentially significant shortfall of the SMM for unsteady flows. In particular, measuring the 'true' transition matrix, that is, the one that homogenizes as more and more pulses are included, is very computationally expensive as it requires high-resolution simulations that track many particles across many initial conditions. This becomes so computationally expensive that its effort compares to running a direct numerical simulation of the full microscale system, thus somewhat defeating the purpose of an upscaled model, particularly given that the USM appears to work quite well.

5 Results

In the previous section we focused on parameterizing variants of the ADE, uncorrelated spatial model and spatial Markov models looking at results from the lowest and highest Reynolds number that we considered (Re = 15 and Re = 280). Here we focus on the best variants of each model and compare results from each model for a variety of Reynolds numbers spanning this range. Recall that the best variants of the models were: the ADE with a transient dispersion coefficient, the USM with $\xi_* = 2$, and the SMM with $\beta = 25$ for steady flow and $\beta = 2$ for unsteady flow.

Figure 14 compares the three models' predictions of the second centered moment of the solute plume to the actual data from the microscale simulations. As before, since we used $\sigma^2(t)$ to parameterize the ADE, the model predicts plume spreading perfectly in both steady and unsteady flows. For the steady flows the spatial Markov model (recall with 25 bins) significantly outperforms the uncorrelated spatial model and is close to the result from the microscale simulation. For the unsteady flows, however, the uncorrelated spatial model gives similar predictions to the other two models, outperforming the spatial Markov model in the highest Reynolds number case. Recall that for unsteady flows the spatial Markov model only uses 2 bins as the higher bin case fails completely.

Figure 15 compares the same three models' predictions of breakthrough curves, $f_{S_\xi}(t)$ for $\xi = 10, 100$, and 1000 to the microscale data. For the steady flows, the ADE model underpredicts the peak concentration at pre-asymptotic spatial locations and significantly overpredicts the width of the breakthrough curves, while the uncorrelated spatial model does the opposite—it overpredicts the peak concentration and underpredicts the width of the breakthrough curves. In all three steady cases the spatial Markov model appears to outper-

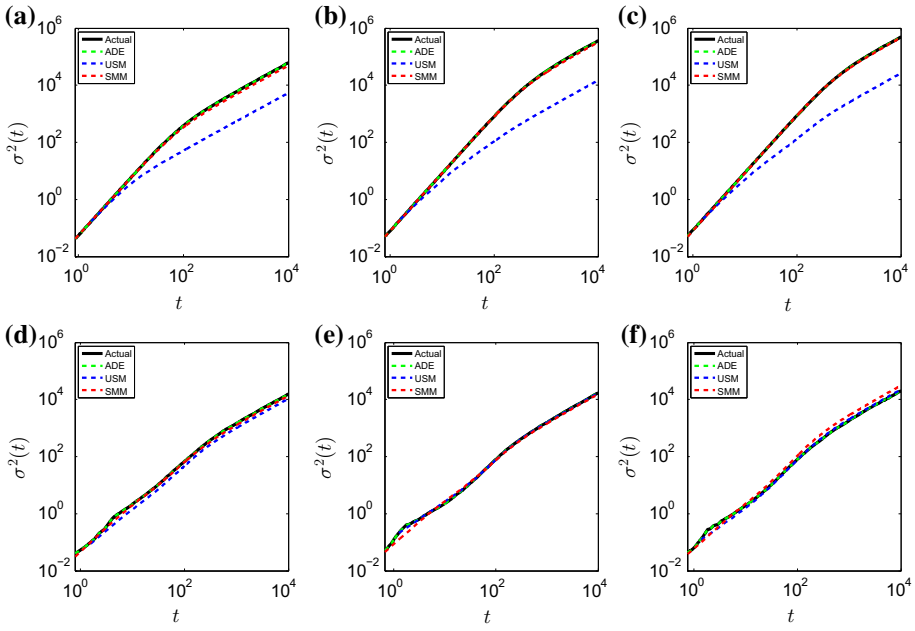

Fig. 14 ADE, uncorrelated spatial model and Spatial Markov model predictions of $\sigma^2(t)$ for steady flow: **a** Re = 15, **b** Re = 60, **c** Re = 80 and unsteady flow: **d** Re = 115, **e** Re = 145, **f** Re = 280

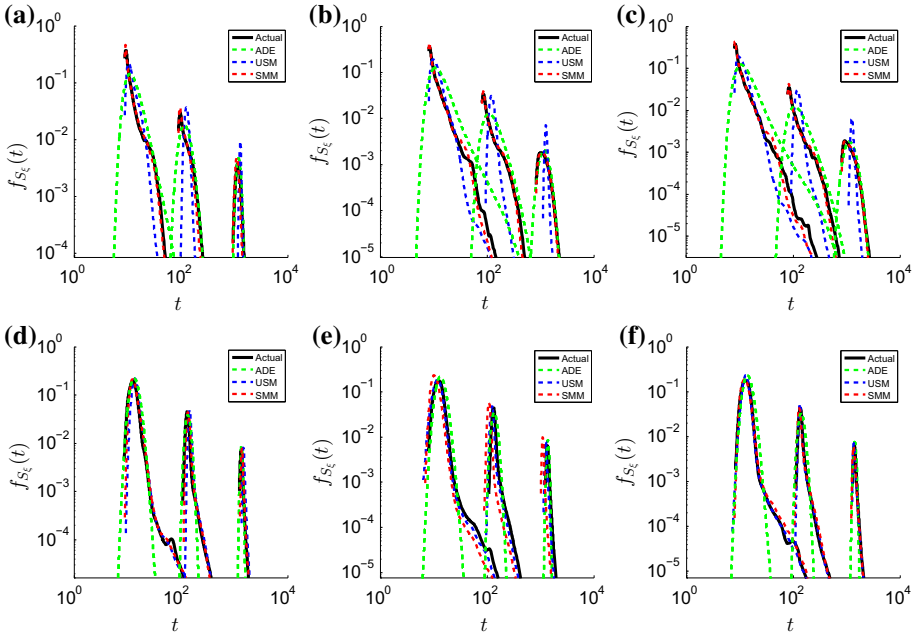

Fig. 15 ADE, uncorrelated spatial model and spatial Markov model predictions of breakthrough curves, $f_{S_\xi}(t)$, at $x = \xi L$ for $\xi = 10$, 100, and 1000 for steady flow: **a** Re = 15, **b** Re = 60, **c** Re = 80 and unsteady flow: **d** Re = 115, **e** Re = 145, **f** Re = 280

form the other two models, closely matching the breakthrough curves, including features such as non-monotonically decreasing tails, except perhaps at the greatest downstream distances where the ADE appears to perform quite well, as one might expect given that at asymptotic times it is a valid upscaled model. This suggests that the inclusion of correlation is critical to the accurate upscaling of transport through these domains under steady flow conditions.

The unsteady flow cases tell a different story. Here both of the spatial models do a similar job in matching the measured breakthrough curves, including matching peak concentrations and tails. Arguably even the ADE does a relatively good job, although it fails to capture tails in the breakthrough curves at the smaller distances. Thus, for these cases, depending on the application and question in mind (e.g., if short distance tails are deemed unimportant), the ADE may be well suited as an upscaled model as long as the transient evolution of the dispersion coefficient can be modeled adequately. If such features are deemed important, an uncorrelated spatial model, which is easier to implement than its Markovian counterpart, will suffice.

To put a more quantitative measure on these more qualitative descriptions Table 1 ranks each of the upscaled models ability to reproduce the breakthrough curves measured from the fully resolved simulations, relative to one another. Results for all of the Reynolds numbers and three downstream distances are shown. The ranking is based on mean absolute error of the cumulative breakthrough $MAE = \frac{1}{N}\sum_{i=1}^{N} |modeled_i - actual_i|$. Other measures were also considered, resulting in a similar ranking. Table 1 clearly shows that in all but one of the steady flow cases (Re = 15, 60 and 80) the spatial Markov model outperforms the other two. The one instance where this does not happen is for Re = 15 at the biggest downstream

Table 1 Table ranking the model predictions of breakthrough curves relative to the highly resolved data for all Reynolds numbers and distance $x = 10L$,$100L$ and $1000L$

	Re = 15	Re = 60	Re = 80
$x = 10L$	S, A, U $(1, 16, 18) \times 10^{-4}$	S, U, A $(1, 14, 28) \times 10^{-4}$	S, U, A $(6, 12, 110) \times 10^{-5}$
$x = 100L$	S, A, U $(6, 1740) \times 10^{-5}$	S, A, U $(8, 130, 240) \times 10^{-5}$	S, A, U $(1, 3, 60) \times 10^{-5}$
$x = 1000L$	A, S, U $(6, 20, 110) \times 10^{-5}$	S, A, U $(7, 78, 130) \times 10^{-5}$	S, A, U $(3, 13, 50) \times 10^{-5}$
	Re = 115	Re = 145	Re = 280
$x = 10L$	S, U, A $(4, 10, 20) \times 10^{-4}$	U, A, S $(5, 15, 21) \times 10^{-4}$	U, S, A $(5, 6, 17) \times 10^{-4}$
$x = 100L$	U, S, A $(4, 16, 23) \times 10^{-4}$	U, A, S $(9, 13, 29) \times 10^{-4}$	U, S, A $(4, 9, 23) \times 10^{-4}$
$x = 1000L$	A, U, S $(4, 7, 14) \times 10^{-4}$	U, A, S $(3, 10, 24) \times 10^{-4}$	U, A, S $(3, 3, 5) \times 10^{-4}$

The rank is based on mean absolute error $MAE = \frac{1}{N}\sum_{i=1}^{N} |modeled_i - actual_i|$ and the sequences are presented from lowest to highest MAE
U uncorrelated spatial model, *S* the spatial Markov model, *A* the advection dispersion equation

distance, where it is likely that the ADE matches so well because the system has reached an asymptotic state where Taylor dispersion ideas hold and the asymptotic ADE is valid, in which case it is perhaps the most obvious choice of model given that it is the easiest to implement. For all of the lower Reynolds number cases the MAE for the spatial Markov model was at least 1–2 orders of magnitude smaller than for the uncorrelated spatial model. For the lowest unsteady Reynolds number there is no clear winner as each of the three models appears to be best depending on the downstream distance, perhaps reflecting that this Reynolds number lies in a transition regime where no clear model should win. For the highest unsteady Reynolds numbers (Re = 145 and 280) the uncorrelated spatial model appears to consistently perform best, although for the highest Reynolds number case at biggest distance $x = 1000L$ the ADE compares almost as favorably.

A key question that arises is: Why are correlation effects important for the lower Reynolds number steady flows, but less important for the larger Reynolds number unsteady cases? While the aforementioned Fig. 10 already schematically illustrates in a qualitative sense the physical mechanism behind why correlation effects will persist in steady flows, but not unsteady ones, it does not explicitly quantify it. To address this, let us define two transition velocities,

$$v_{\tau_i} = \frac{L}{\tau_i}, \quad v_{x_i} = \frac{\Delta x_i}{L/\bar{u}}. \tag{20}$$

v_{τ_i} defines the characteristic velocity with which a particle traverses a periodic element given its transition time τ_i. v_{x_i} characterizes the characteristic velocity of a particle over mean advective time $L/\bar{u}$ given that it has travelled a distance Δx_i. We can now, using our microscale model, calculate the correlation of v_τ with distance (over multiple jumps of length L) and the correlation of v_x over time (over multiple time steps of size $L/\bar{u}$). Plots of the correlations are shown for the steady Re = 15 and unsteady Re = 280 cases in Fig. 16. The low Reynolds number case shows long-range correlation over space and time, although shorter correlation length in space than in time, which justifies the choice of fixing jump length with random time step in the spatial model framework. While these correlations appear to be exponential, their range is large enough that correlation effects must be included in the spatial model. On the other hand, for the unsteady flow, the correlation in time drops sharply

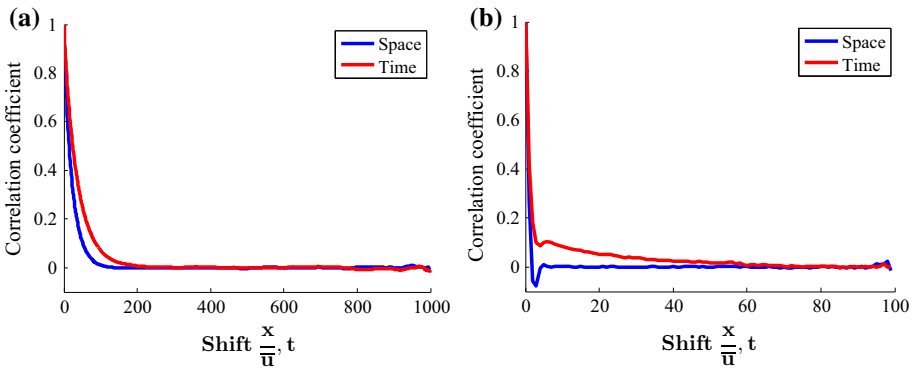

Fig. 16 Velocity correlation in space and time for different Reynolds numbers. Steady flow: **a** Re = 15, Pe = 7.5×10^3 Unsteady flow: **b** Re = 280, Pe = 1.4×10^5. Note the difference in scale on the x-axis

and then persists over long times, while the correlation in space drops almost immediately to zero, demonstrating why no correlation effects need be included in the spatial model for these cases.

6 Conclusions

We simulated flow and transport through an idealized porous medium using high-resolution microscale numerical simulations over a range of Reynolds numbers that spanned the steady inertial and unsteady flow regimes. These simulations provided the data needed to parameterize and validate three upscaled pre-asymptotic transport models—an ADE with a transient dispersion coefficient, an uncorrelated spatial model with fixed space step and travel time distribution, and a spatial Markov model with fixed space step and joint travel time distribution. The goal was to verify the three models' ability to predict two common transport metrics—the second centered moment of a solute plume and breakthrough curves, both originating from pulse initial conditions. We focused primarily on the ability of the models to predict these features at pre-asymptotic spatial and temporal scales, since these models were specifically designed to capture the more difficult to predict pre-asymptotic transport regime and the use of upscaled models to predict asymptotic transport is well established.

Broadly speaking, our conclusions can be divided among two predominant flow regimes, the inertial steady and unsteady regimes. In the inertial steady flow regime:

1. Due to the use of a Schmidt number representative of solutes in water, diffusive effects were very small relative to advective effects for the range of Reynolds numbers considered. These small diffusive effects suggest large pre-asymptotic time and length scales, as it is diffusion that sets these scales. This led to persistent non-Fickian behavior of the solute plume over a large range of the simulated time scales, consistent with observations and conclusions from previous studies.
2. Due to the strong Lagrangian velocity correlations in space that arise due to weak diffusive effects, the spatial Markov model was the only model that was able to accurately describe both the evolution of the second centered moment in time and the non-Fickian details of the breakthrough curves, such as non-monotonic post-peak breakthrough curves and tails at early times. This indicates that when flows are steady and Peclet numbers large,

it is critical to account for velocity correlation in effective upscaled models, of the type presented here (i.e., fixed spatial step), that should mimic small-scale behaviors.
3. The ADE with a transient dispersion coefficient failed to adequately capture the peak and tail of the non-Fickian breakthrough curves at pre-asymptotic times, indicating that the use of a transient dispersion coefficient is not sufficient to accurately model the pre-asymptotic physics, again consistent with previous studies.
4. The uncorrelated spatial model failed to adequately reproduce either of the transport metrics due to its inability to enforce the tendency of particles that travel along fast streamlines to persist along fast streamlines and of slow ones to persist along slow paths. This reaffirms that in steady flows it is crucial to account for velocity correlation in upscaled models at pre-asymptotic length scales.

In the unsteady flow regime:

1. Despite high Peclet numbers and thus small diffusive effects, unsteadiness in the flow appears to lead to a rapid decorrelation in particle velocities in space; however, velocity correlation in time persisted over longer scales, thus suggesting the strength of an uncorrelated spatial model over an effective ADE at shorter scales.
2. All three of the models, when optimally chosen, were able to accurately predict the second centered moment of the plume and the peaks of the breakthrough curves. This indicates that an upscaled model which accounts for the correlation structure and the shape of the travel time distribution is unnecessary to predict these metrics.
3. Both spatial models were able to capture tailing in the breakthrough curves. However, the ADE failed in doing so. Thus, if tailing features are deemed important, a model which accounts for the shape of the travel time distribution is required. However, if tailing is deemed unimportant, the ADE performs well.
4. The spatial Markov model only worked well when a small number of bins to discretize the transition matrix were used. When a large number of bins were used the model yielded unphysical results. This appears to be an artifact of how the transition matrix is measured, that is, from a single-pulse initial condition, which is unable to capture the complete correlation structure inherent to the flow. If the transition matrix is measured from multiple pulses injected at different times it appears to homogenize more and more as the number of pulses increases. However, the computational cost associated with measuring this transition matrix can become so expensive as to be comparable to a full microscale simulation, thus defeating the purpose of an upscaling exercise. However, this apparent homogenization of the transition matrix does explain why the USM appears to work well for the unsteady flows as it corresponds to a completely uniform transition matrix where all bins are equally accessible by all particles.

Thus, generally speaking, when flows are steady we recommend the use of a model which accounts for velocity correlation, like the spatial Markov model, to upscale transport at pre-asymptotic times. As the Reynolds numbers become larger and the flow becomes unsteady, it appears sufficient to use an upscaled model which is parameterized with either a single breakthrough curve or a time series of the first and second spatial moments of the solute plume. One of the benefits of the uncorrelated spatial model is that the effective asymptotic transport coefficients can be predicted entirely from the transition time distribution (e.g., Shlesinger 1974; Margolin and Berkowitz 2002), meaning that transport can be well predicted all the way from pre-asymptotic to asymptotic times. Therefore, as the velocity fields where transport occurs get more complicated (by becoming unsteady), the transport upscaling process becomes simpler, allowing us to use models that require less information.

Acknowledgments This material is based upon work supported by, or in part by, the US Army Research Laboratory and the US Army Research Office under Contract/Grant number W911NF1310082. DB and NS would also like to acknowledge partial funding from NSF Grant EAR-1351625. Any opinions, findings, conclusions or recommendations do not necessarily reflect the views of the funding agencies. The computations in this work were supported by the Notre Dame Center for Research Computing. The helpful comments of two anonymous reviewers are gratefully acknowledged.

References

Aris, R.: On the dispersion of a solute in a fluid flowing through a tube. Proc. R. Soc. Lond. Math. Phys. Sci. **235**(1200), 67–77 (1956)

Bachu, S.: Screening and ranking of sedimentary basins for sequestration of CO2 in geological media in response to climate change. Environ. Geol. **44**(3), 277–289 (2003)

Benson, D.A., Wheatcraft, S.W., Meerschaert, M.M.: The fractional-order governing equation of Lévy motion. Water Resour. Res. **36**(6), 1413–1423 (2000)

Berkowitz, B., Klafter, J., Metzler, R., Scher, H.: Physical pictures of transport in heterogeneous media: advection–dispersion, random-walk, and fractional derivative formulations. Water Resour. Res. **38**(10), 1–9 (2002)

Berkowitz, B., Cortis, A., Dentz, M., Scher, H.: Modeling non-Fickian transport in geological formations as a continuous time random walk. Rev Geophys **44**(2) (2006)

Bolster, D., Mheust, Y., Borgne, T.L., Bouquain, J., Davy, P.: Modeling preasymptotic transport in flows with significant inertial and trapping effects—the importance of velocity correlations and a spatial Markov model. Adv. Water Resour. **70**, 89–103 (2014)

Bouquain, J., Méheust, Y., Bolster, D., Davy, P.: The impact of inertial effects on solute dispersion in a channel with periodically varying aperture. Phys. Fluids **24**(8), 083,602 (2012)

Brenner, H.: Dispersion resulting from flow through spatially periodic porous media. Philos. Trans. R. Soc. Lond. Math. Phys. Sci. **297**(1430), 81–133 (1980)

Cardenas, M.B.: Three-dimensional vortices in single pores and their effects on transport. Geophys. Res. Lett. **35**(18) (2008). doi:10.1029/2008GL035343

Cardenas, M.B., Slottke, D.T., Ketcham, R.A., Sharp, J.M.: Effects of inertia and directionality on flow and transport in a rough asymmetric fracture. J. Geophys. Res. Solid. Earth (1978–2012) **114**(B6) (2009). doi:10.1029/2009JB006336

Chaudhary, K., Cardenas, M.B., Deng, W., Bennett, P.C.: The role of eddies inside pores in the transition from Darcy to Forchheimer flows. Geophys. Res. Lett. **38**(24) (2011)

Chaudhary, K., Cardenas, M.B., Deng, W., Bennett, P.C.: Pore geometry effects on intrapore viscous to inertial flows and on effective hydraulic parameters. Water Resour. Res. **49**(2), 1149–1162 (2013)

Cushman, J.H., Ginn, T.R.: Fractional advection-dispersion equation: a classical mass balance with convolution-Fickian flux. Water Resour. Res. **36**(12), 3763–3766 (2000)

de Anna, P., Le Borgne, T., Dentz, M., Tartakovsky, A.M., Bolster, D., Davy, P.: Flow intermittency, dispersion, and correlated continuous time random walks in porous media. Phys. Rev. Lett. **110**, 184502 (2013). doi:10.1103/PhysRevLett.110.184502

Delgado, J.: Longitudinal and transverse dispersion in porous media. Chem. Eng. Res. Des **85**(9), 1245–1252 (2007)

Dentz, M., Berkowitz, B.: Transport behavior of a passive solute in continuous time random walks and multirate mass transfer. Water Resour. Res. **39**(5) (2003). doi:10.1029/2001WR001163

Dentz, M., Bolster, D.: Distribution-versus correlation-induced anomalous transport in quenched random velocity fields. Phys. Rev. Lett. **105**(24), 244,301 (2010)

Dentz, M., Kinzelbach, H., Attinger, S., Kinzelbach, W.: Temporal behavior of a solute cloud in a heterogeneous porous medium: 1. Point-like injection. Water Resour. Res. **36**(12), 3591–3604 (2000)

Dentz, M., Cortis, A., Scher, H., Berkowitz, B.: Time behavior of solute transport in heterogeneous media: transition from anomalous to normal transport. Adv. Water Resour. **27**(2), 155–173 (2004)

Edery, Y., Guadagnini, A., Scher, H., Berkowitz, B.: Origins of anomalous transport in heterogeneous media: structural and dynamic controls. Water Resour. Res. **50**(2), 1490–1505 (2014)

Fitts, C.R.: Uncertainty in deterministic groundwater transport models due to the assumption of macrodispersive mixing: evidence from the Cape Cod (Massachusetts, USA) and Borden (Ontario, Canada) tracer tests. J Contam. Hydrol. **23**(1), 69–84 (1996)

Freund, H., Zeiser, T., Huber, F., Klemm, E., Brenner, G., Durst, F., Emig, G.: Numerical simulations of single phase reacting flows in randomly packed fixed-bed reactors and experimental validation. Chem. Eng. Sci. **58**(3), 903–910 (2003)

Germano, M., Piomelli, U., Moin, P., Cabot, W.: A dynamic subgrid-scale eddy viscosity model. Phys. Fluids A **3**, 1760 (1991)
Haggerty, R., Gorelick, S.M.: Multiple-rate mass transfer for modeling diffusion and surface reactions in media with pore-scale heterogeneity. Water Resour. Res. **31**(10), 2383–2400 (1995)
Hornung, U.: Homogenization and Porous Media, Interdisciplinary Applied Mathematics, vol. 6. Springer, New York (1997)
Kang, P.K., Dentz, M., Le Borgne, T., Juanes, R.: Spatial Markov model of anomalous transport through random lattice networks. Phys. Rev. Lett. **107**(180), 602 (2011). doi:10.1103/PhysRevLett.107.180602
Kees, C., Farthing, M., Fong, M.: Locally conservative, stabilized finite element methods for a class of variable coefficient Navier-Stokes equations. Technical Report TR-09-12, U.S. Army Engineer Research and Development Center, Coastal and Hydraulics Laboratory (2009)
Le Borgne, T., Dentz, M., Carrera, J.: Lagrangian statistical model for transport in highly heterogeneous velocity fields. Phys. Rev. Lett. **101**(9), (2008a). doi:10.1103/PhysRevLett.101.090601
Le Borgne, T., Dentz, M., Carrera, J.: Spatial Markov processes for modeling Lagrangian particle dynamics in heterogeneous porous media. Phys. Rev. E **78**(2), (2008b). doi:10.1103/PhysRevE.78.026308
Le Borgne, T., Bolster, D., Dentz, M., Anna, P., Tartakovsky, A.: Effective pore-scale dispersion upscaling with a correlated continuous time random walk approach. Water Resour. Res. **47**(12) (2011). doi:10.1029/2011WR010457
Margolin, G., Berkowitz, B.: Spatial behavior of anomalous transport. Phys. Rev. E **65**(3), 031,101 (2002)
Margolin, G., Dentz, M., Berkowitz, B.: Continuous time random walk and multirate mass transfer modeling of sorption. Chem. Phys. **295**(1), 71–80 (2003)
Mattis, S.A., Dawson, C.N., Kees, C.E., Farthing, M.W.: Numerical modeling of drag for flow through vegetated domains and porous structures. Adv. Water Resour. **39**, 44–59 (2012)
Meerschaert, M.M., Zhang, Y., Baeumer, B.: Tempered anomalous diffusion in heterogeneous systems. Geophys. Res. Lett. **35**(17) (2008). doi:10.1029/2008GL034899
Meneveau, C., Lund, T.: The dynamic Smagorinsky model and scale-dependent coefficients in the viscous range of turbulence. Phys. Fluids **9**, 3932 (1997)
Mills, A.F.: Basic Heat and Mass Transfer, vol. 2. Prentice Hall, Upper Saddler River (1999)
Montroll, E.W., Weiss, G.H.: Random walks on lattices. ii. J Math. Phys. **6**(2), 167–181 (1965)
Nepf, H., Mugnier, C., Zavistoski, R.: The effects of vegetation on longitudinal dispersion. Estuar. Coast. Shelf Sci. **44**(6), 675–684 (1997)
Neuman, S.P., Tartakovsky, D.M.: Perspective on theories of non-Fickian transport in heterogeneous media. Adv. Water Resour. **32**(5), 670–680 (2009)
Richmond, M.C., Perkins, W.A., Scheibe, T.D., Lambert, A., Wood, B.D.: Flow and axial dispersion in a sinusoidal-walled tube: effects of inertial and unsteady flows. Adv. Water Resour. **62**, 215–226 (2013)
Risken, H.: Fokker–Planck Equation. Springer, New York (1984)
Scher, H., Lax, M.: Stochastic transport in a disordered solid. i. Theory. Phys. Rev. B **7**, 4491–4502 (1973). doi:10.1103/PhysRevB.7.4491, http://link.aps.org/doi/10.1103/PhysRevB.7.4491
Schumer, R., Benson, D.A., Meerschaert, M.M., Baeumer, B.: Multiscaling fractional advection-dispersion equations and their solutions. Water Resourc. Res. **39**(1) (2003). doi:10.1029/2001WR001229
Shlesinger, M.F.: Asymptotic solutions of continuous-time random walks. J. Stat. Phys. **10**(5), 421–434 (1974)
Taylor, G.: Dispersion of soluble matter in solvent flowing slowly through a tube. Proc. R. Soc. Lond. Math. Phys. Sci. **219**(1137), 186–203 (1953)
Vilarrasa, V., Bolster, D., Dentz, M., Olivella, S., Carrera, J.: Effects of CO2 compressibility on CO2 storage in deep saline aquifers. Transp. Porous Media **85**(2), 619–639 (2010)
Voke, P.: Subgrid-scale modelling at low mesh Reynolds number. Theor. Comput. Fluid Dyn. **8**(2), 131–143 (1996)
Wen, Z., Huang, G., Zhan, H.: Non-Darcian flow in a single confined vertical fracture toward a well. J. Hydrol. **330**(3), 698–708 (2006)
Whitaker, S.: The Method of Volume Averaging, vol. 13. Springer, New York (1998)
White, B.L., Nepf, H.M.: Scalar transport in random cylinder arrays at moderate Reynolds number. J Fluid Mech. **487**, 43–79 (2003)
Wood, B.D.: Inertial effects in dispersion in porous media. Water Resour. Res. **43**(12) (2007). doi:10.1029/2006WR005790